ELSEVIER

Physica C 260 (1996) 8–18

PHYSICA C

AC response of the vortex liquid in the high-T_c superconducting cylinder

Chien-Jang Wu, Tseung-Yuen Tseng

Department of Electronics Engineering and Institute of Electronics, National Chiao-Tung University, Hsinchu, Taiwan

Received 19 January 1996

Abstract

The ac response of the vortex liquid of a high-T_c superconducting cylinder in the parallel field configuration is examined theoretically. The ac properties are analyzed from the associated complex ac permeability calculated on the basis of hydrodynamics theory. The permeability is primarily dominated by two frequency-dependent penetration lengths which are also shown to be independent of the geometries considered. In the simple flux-flow regime, the second peak in ac loss is observed to be enhanced while the first peak is depressed for the superconducting cylinder. In the viscous flux liquid, the ac response is found to rely on the viscosity, ratio of shear modulus to nonlocal compressional modulus, and the geometries discussed. The results indicate some basic difference in ac permeabilities between superconducting cylinder and slab.

Keywords: Mixed state; Penetration depth,; Type II superconductors; Flux lattice

1. Introduction

The discovery of high-T_c superconductors (HTSC) has revived the study of vortex response to the ac field in these high-κ superconductors. The investigation of the ac response in the mixed state can be alternatively used to understand the vortex dynamics. At present, the measurements of vortex response are performed by ac techniques such as the vibrating-reed mechanical resonator [1], surface impedance [2–4], and ac magnetic permeability [5]. All these techniques have the common feature that a small alternating magnetic field is superimposed to a steady field. In the linear response regime, the ac response is independent of the amplitude of the alternating field. The ac field is applied parallel to the surface of the superconductor which in turn generates screening currents near the surface. The currents then produce a Lorentz force acting on the vortices and cause an oscillation of vortices. The oscillating vortices propagate into the interior of the superconductor due to the vortex interaction. The moving vortices are, however, impeded by some friction or pinning. Hence vortex dynamics strongly influences the ac properties of type-II superconductors, for instance, the ac permeability or the surface impedance, which are widely considered both experimentally and theoretically.

Much effort has been made to investigate theoretically the electromagnetic response of a vortex system in high-T_c superconductors. A unified theory of the effects of vortex pinning, flux creep and flow on the surface impedance and rf magnetic permeability of isotropic type-II superconductors has been developed by Coffey and Clem [6-8]. The vortex dynamics is treated self-consistently and a complex ac penetration depth is calculated to study the high-frequency vortex

PII S0921-4534(96)00109-8

response. The dissipation peak occurs when the complex penetration depth is of the order of the sample size and is usually ascribed to the skin size effect [9,10] based on the model of thermally activated depinning of vortex lines. For a pinned vortex solid, Koshelev and Vinour [11] investigated the frequency response within the framework of the collective pinning theory. They have incorporated the thermal fluctuation into the Campbell theory. Based on the thermally activated flux flow (TAFF) model [12,13], Yeh [14] studied the high-frequency vortex response near the depinning threshold. A discussion of linear ac response in the mixed state from the unique macroscopic viewpoint has also been given by van der Beek et al. [15].

The ac techniques are also very useful in the determination of the irreversibility line in the (H,T) phase diagram of the disordered HTSC [16]. The (H,T) phase diagram, however, exhibits a large region where the vortex lattice is in a liquid phase [17], i.e., the vortex-liquid. Therefore the ac response of the vortex liquid on the TAFF basis appears to be no longer useful, since the TAFF theory does not completely incorporate the vortex-vortex interaction. The ac response of flux-line liquid has recently been considered within the framework of hydrodynamics by Chen and Marchetti [18]. The hydrodynamic treatment has incorporated the viscoelastic nonlocality effect arising from intervortex interaction and entanglement. The ac permeability of a slab and surface impedance of an semi-infinite sample have been given in Ref. [18].

In this paper, we extend the work of Chen and Marchett [18] and calculate the ac response of the vortex liquid in the superconducing cylinder. As customary, the most commonly used geometries for ac or microwave response in HTSC are the slab and cylinder. The calculated complex ac permeabilities for slab and cylinder in various approaches are now available [12,19]. It is therefore of interest to calculate the corresponding permeability for a cylinder in the vortex liquid state which has not been seen thus far. We also illustrate some basic difference in both real and imaginary parts of permeabilities for the slab and cylinder. The problem considered here is applicable in the microwave cavity perturbation experiment especially in the parallel field configuration [20].

2. Basic equations

We consider a uniaxial type-II superconducting cylinder (assumed to be infinitely long) with axis in the z-direction and cross section parallel to x–y plane. For high-T_c cuprate, the c-axis is chosen as the z-direction and the a–b plane as the x–y plane. A static magnetic field $\boldsymbol{H} = \hat{z}H$ is applied parallel to the surface of cylinder to generate the vortex array. The density of vortices n_0 and the average flux density $\boldsymbol{B}_0 = \hat{z}B_0$ are related by $n_0 = B_0/\phi_0$ and $a_0 \approx 1/\sqrt{n_0}$, where ϕ_0 is the flux quantum defined by $\phi_0 = hc/2e$ and a_0 is the intervortex spacing.

In this paper, we are interested in the regime $H_{c1} \ll B \ll H_{c2}$, namely, $\xi_{ab} \ll a_0 \ll \lambda_{ab}$, where ξ_{ab} and λ_{ab} are the coherence and penetration lengths in the a–b plane, respectively. In the parallel configuration, the demagnetization factor is ignored so that $B_0 \approx H$. We assume the vortex array is in a liquid phase and the vortex dynamics is described by some hydrodynamic fields coarse-grained over several lattice spacings.

The electrodynamics of a superconductor is well described by Maxwell's equations

$$\nabla \times \boldsymbol{e} = -\frac{1}{c}\frac{\partial \boldsymbol{b}}{\partial t} \tag{1}$$

$$\nabla \times \boldsymbol{b} = \frac{4\pi}{c}\boldsymbol{j} + \frac{1}{c}\frac{\partial \boldsymbol{e}}{\partial t} \tag{2}$$

$$\nabla \cdot \boldsymbol{e} = 4\pi\rho \tag{3}$$

$$\nabla \cdot \boldsymbol{b} = 0, \tag{4}$$

two-fluid equation

$$\boldsymbol{j} = \boldsymbol{j}_n + \boldsymbol{j}_s, \tag{5}$$

and London equation in the presence of vortices, [18]

$$\nabla \times \boldsymbol{\Lambda} \cdot \boldsymbol{j}_s = \frac{c}{4\pi}(-\boldsymbol{b} + \phi_0 \boldsymbol{T}), \tag{6}$$

where $\boldsymbol{e}$ and $\boldsymbol{b}$ are the local fields, $\boldsymbol{j}_s$ the supercurrent, $\boldsymbol{j}_n$ the normal current specified by $\boldsymbol{j}_n = \sigma_n \boldsymbol{e}$, $\boldsymbol{\Lambda}$ is a diagonal tensor with elements $\Lambda_{xx} = \Lambda_{yy} = \lambda_{ab}^2$ and $\Lambda_{zz} = \lambda_c^2$, and $\boldsymbol{T}$ is defined by $\boldsymbol{T} = \hat{z}n + \boldsymbol{\tau}$ with n and $\boldsymbol{\tau}$ the coarse-grained hydrodynamic density and tilt fields of the vortex array, respectively. By making use of the above equations, one easily has

$$\nabla \times \boldsymbol{\Lambda} \cdot \nabla \times \boldsymbol{b} = -\boldsymbol{b} + \phi_0 \boldsymbol{T} - \frac{4\pi\sigma_n\lambda^2}{c^2}\frac{\partial \boldsymbol{b}}{\partial t} \quad . \tag{7}$$

In obtaining the Eq. (7), we have dropped the term arising from displacement current density because the ac response considered in this context is restricted to frequencies no higher than microwave.

In addition to the above-described equation, to investigate the response of the vortex liquid to the ac field, we include some hydrodynamic equations to describe the vortex dynamics. For the linear response regime, the linearized hydrodynamic equations are given by [18]

$$\partial\, \delta n/\partial t + n_0 \nabla_\perp \cdot \boldsymbol{v} = 0, \tag{8}$$

$$-\gamma \boldsymbol{v} + \eta_s \nabla_\perp^2 \boldsymbol{v} + \eta_b \nabla_\perp (\nabla_\perp \cdot \boldsymbol{v}) + \eta_z \frac{\partial^2 \boldsymbol{v}}{\partial z^2} - \frac{1}{c} \boldsymbol{B}_0 \times \boldsymbol{j} = 0. \tag{9}$$

Eq. (8) in fact is the equation of continuity for the areal density of vortices with $\delta n = n - n_0$, the deviation from the equilibrium value, n_0. Eq. (9) behaves as an equation of motion for the moving vortex with velocity $\boldsymbol{v}$, and friction coefficient γ. The coefficients, η_s, η_b, and η_z are the shear, bulk, and tilt viscosity constants, respectively. A detailed description of the viscosity coefficients can be found in Ref. [18]. Eqs. (7)–(9) serve as the foundation for investigating the ac response of the flux-line liquid in type-II superconductors.

3. Calculation and discussion of ac permeability for a cylinder

We now consider the above configuration for a cylinder with radius a in cross sectional area. An ac field $\boldsymbol{H}_a = \hat{z}\delta H_a e^{iwt}$ is applied parallel to the surface of the cylinder (also parallel to $\boldsymbol{H}$), with $\delta H_a \ll H$. The local field $\boldsymbol{b}$ in Eq. (7) is thus assumed to be $\boldsymbol{b} = \hat{z}\delta B_z(\rho) e^{iwt}$ and $\tau = 0$ since the vortex lines are on average aligned along the z-direction. Eq. (7) in this case becomes

$$-\frac{1}{\rho}\frac{d}{d\rho}\left(\rho \frac{d\delta B_z}{d\rho}\right) + \left(\frac{1}{\lambda^2} + \frac{1}{\lambda_{nf}^2}\right)\delta B_z = \frac{\phi_0}{\lambda^2}\delta n(\rho), \tag{10}$$

where we have denoted the London penetration length λ_{ab} as λ for simplicity, and λ_{nf} is the normal-fluid skin depth given by $\lambda_{nf}^{-2} = 4\pi i w \sigma_n / c^2$. On the other hand, Eqs. (8) and (9) can be expressed as

$$iw\delta n - n_0 \frac{1}{\rho}\frac{d}{d\rho}(\rho v_\rho) = 0, \tag{11}$$

$$\gamma v_\rho - \tilde{\eta}_\ell \frac{d}{d\rho}\left(\frac{1}{\rho}\frac{d}{d\rho}(\rho v_\rho)\right) + \frac{B_0}{c} j_\theta = 0, \tag{12}$$

where we have used the velocity of moving vortex as $v = -\hat{\rho} v_\rho(\rho)$, and $\tilde{\eta}_\ell = \eta_s + \eta_b$ is the wavevector and frequency-dependent longitudinal viscosity given by Ref. [18],

$$\tilde{\eta}_\ell(q, w) = \frac{\eta_\ell}{1 + iw\tau_\ell(q)}, \tag{13}$$

with static viscosity $\eta_\ell = \tilde{\eta}_\ell$, $(q = 0, w = 0)$ and characteristic relaxation time τ_ℓ. In the case of $w \gg 1/\tau_\ell$, the hydrodynamic theory reduces to the continuum elasticity for the vortex lattice system, correspondingly [18],

$$\tau_\ell = \eta_\ell / [c_{11}(q) + G - c_L(q)], \tag{14}$$

$$\tau_s = \eta_s / G, \tag{15}$$

where c_{11} and G are the compressional and shear elastic moduli of a vortex line elastic medium, respectively. Also the longitudinal compressional modulus $c_L(q)$ and c_{11} are related to $c_{11}(q) = c_L(q) + c_{66}$ with $c_{66} \approx G \ll c_L(q)$. Here c_{66} is the dispersive shear modulus. The expression for bulk modulus $c_L(q)$ can be found in Ref. [21].

The response to the ac field can be obtained by solving δB_z in Eq. (10). Eq. (10) is solvable with the help of Eqs. (11) and (12) together with the boundary condition $\delta B_z(\rho = a) = \delta H_a$. In this article, we consider two conditions in solving Eq. (10). One is the simplest case with $\tilde{\eta}_\ell = 0$, i.e., the flux-flow regime. The other is the viscous liquid with $\tilde{\eta}_\ell \neq 0$ in which the effect of viscosity on the response can be elucidated.

Let us begin to consider the simple flux flow condition at $\tilde{\eta}_\ell = 0$. By combining Eqs. (2), (11) and (12), we have

$$\delta n(\rho) = \lambda_f \frac{1}{\rho}\frac{d}{d\rho}\left(\rho \frac{d\,\delta B_z}{d\rho}\right), \tag{16}$$

where λ_f is the ac penetration length of a vortex liquid given by $\lambda_f^{-2} = iw\gamma / c_L(0)$ with $c_L(0) = B_0^2/4\pi$. A substitution of Eq. (13) in Eq. (10) yields

$$-\left(1+\frac{\lambda_f^2}{\lambda^2}\right)\frac{1}{\rho}\frac{d}{d\rho}\left(\rho\frac{d\,\delta B_2}{d\rho}\right)+\left(\frac{1}{\lambda^2}+\frac{1}{\lambda_{nf}^2}\right)\delta B_2=0. \tag{17}$$

The solution of Eq. (17) is easily obtained from the boundary condition; the result is

$$\delta B_z(\rho)=\delta H_a I_0(\rho/\lambda_{ac})/I_0(a/\lambda_{ac}), \tag{18}$$

where I_0 is the modified Bessel function of the first kind of order zero, and the complex ac penetration length λ_{ac} is defined by

$$\lambda_{ac}(w)=\left(\frac{\lambda^2+\lambda_f^2}{1+\lambda^2\lambda_{nf}^{-2}}\right)^{1/2}, \tag{19}$$

which is exactly the same as that given in Ref. [18]. It alternatively means that the ac penetration length relies only on the model considered and has nothing to do with the geometry used. By the way, the ac penetration length λ_{ac} given in Eq. (19) is very similar to that developed by Coffey and Clem [7,19] in the absence of creep. The associated complex ac is directly evaluated from the integral

$$\mu(w)=\frac{1}{\pi a^2\delta H_a}\int_0^{2\pi}\int_0^{a}\delta B_z(\rho)\rho\,d\rho\,d\theta, \tag{20}$$

which is given by

$$\mu(w)=2\frac{\lambda_{ac}}{a}\frac{I_1(a/\lambda_{ac})}{I_0(a/\lambda_{ac})}, \tag{21}$$

where I_1 is again the modified Bessel function of the first kind of order one. Here the argument of the modified Bessel function is complex-valued and can be numerically evaluated through the integrals

$$I_0(z)=\frac{1}{\pi}\int_0^{\pi}\cosh(z\cos\theta)\,d\theta, \tag{22}$$

$$I_1(z)=\frac{1}{\pi}\int_0^{\pi}e^{z\cos\theta}\cos\theta\,d\theta. \tag{23}$$

The penetration length in Eq. (19) strongly depends on the frequency of the applied ac field and classified into three regimes by two frequency scales. One is the frequency related to flux diffusion, $w_f=c_L(0)/\gamma\lambda^2$. The other $w_{nf}=c^2/(4\pi\sigma_n\lambda^2)$ is dominated by normal fluid. For $w\ll w_f$, the field penetration is controlled by simple flux flow, and $\lambda_{ac}(w)\approx\lambda_f(w)\sim w^{-1/2}$. In the higher frequency regime, $w_f\ll w\ll w_{nf}$, one has $\lambda_{ac}(w)\approx\lambda$ which indicates the static Messner response with a real penetration length. As the frequency becomes much higher, say $w\gg w_{nf}$, $\lambda_{ac}(w)\approx\lambda_{nf}(w)$ is again proportional to $w^{-1/2}$. The response is thus dominated by the normal fluid. The overall frequency-dependent feature of λ_{ac} is given in Fig. 1 of Ref. [18], and replotted here in Fig. 1 for convenience of discussion. In Fig. 2, we illustrate the ac permeability of the cylinder in Eq. (21) where comparsion with the slab has been made, too. The permeability of a slab with thickness $2a$ was calculated by Chen et al. [18] as

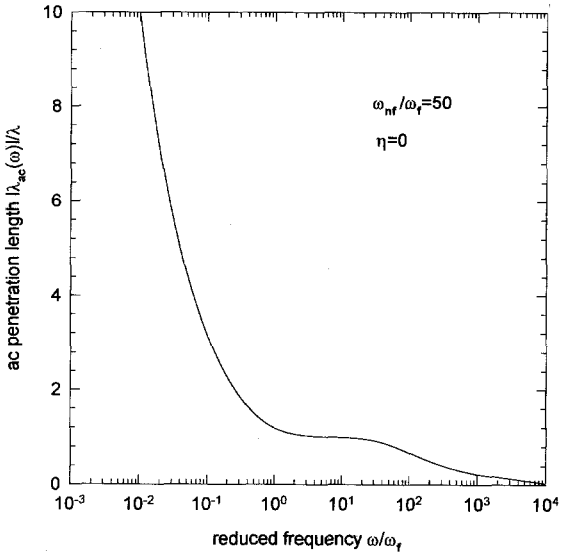

Fig. 1. The normalized complex ac penetration length $|\lambda_{ac}(w)|/\lambda$ in Eq. (19) as a function of reduced frequency w/w_f for the nonviscous vortex liquid with w_{nf}/w_f = 50. Three regimes are identified as described in the text.

$$\mu(w)=(\lambda_{ac}/a)\tanh(a/\lambda_{ac}). \tag{24}$$

As can be seen in Figs. 2a,b, the behavior of $\mu=\mu'-i\mu''$ for the cylinder is somewhat distinc from that of the slab. In Fig. 2a, $a/\lambda=10$, the peak height in μ'' at lower frequency is depressed from 0.417 for the slab to 0.367 for the cylinder, whereas, the second peak height at higher frequency is enhanced. Furthermore, the peak frequencies for the cylinder are in-

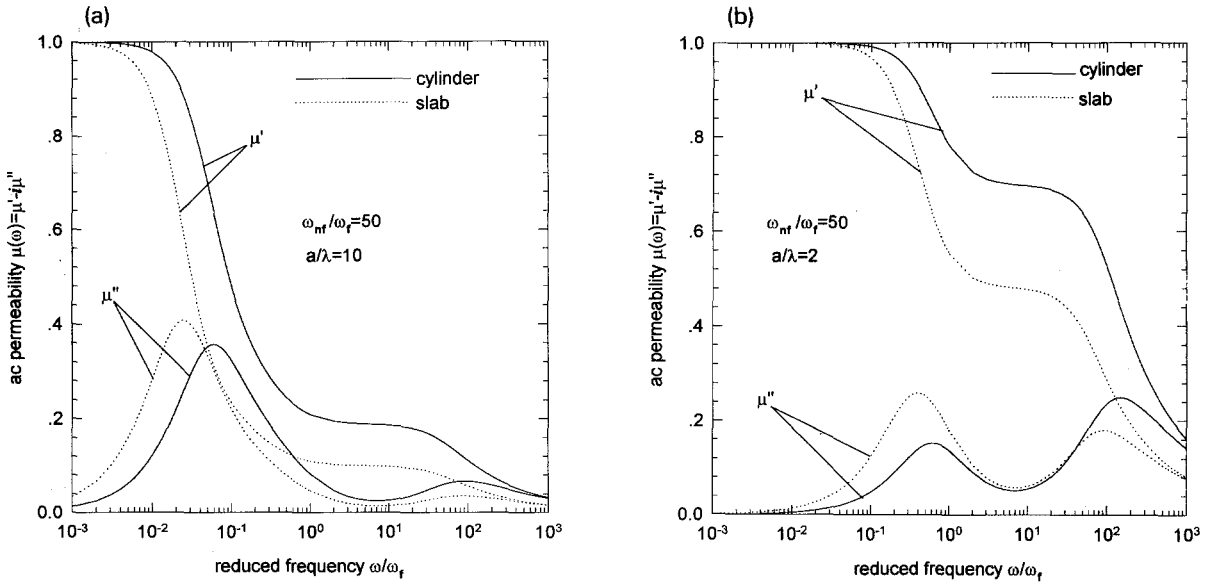

Fig. 2. (a) The real and imaginary parts of ac permeabilities for both cylinder (radius = a) in Eq. (21) and slab (half width = a) in Eq. (24) at $\tilde{\eta} = 0$, $w_{nf}/w_f = 50$ and $a = 10\lambda$. (b) The real and imaginary parts of ac permeabilities for both cylinder (radius = a) and slab (half width = a) at $\tilde{\eta} = 0$, $w_{nf}/w_f = 50$ and $a = 2\lambda$.

creased, especially for the peak located at the lower frequency regime. Another significant feature shown in the cylinder is the disappearance of the coincidence in μ' and μ'' which occurs around $w/f_f \approx 0.1$ for the slab. For the smaller ratio of a/λ, depicted in Fig. 2b, the above features remain observable. Furthermore, the depression in the first peak and the enhancement in second peak of μ'' for the cylinder appears to be more pronounced.

The results shown in Fig. 2 elucidate the main difference arising from the different geometries considered. Concerning the nature of this two-peak behavior in μ'', one is refered to Ref. [18]. Here we only demonstrate the difference due to the geometric effect. The real part, μ' of the cylinder is found to be larger than that of the slab for all frequencies. This signals that the resonance frequency is strongly geometry-dependent, when the superconductor is considered to be a part of the resonant circuit.

We now go on to study the ac response of viscous vortex liquid for a superconducting cylinder. For a viscous liquid, the response due to vortex-vortex interaction and entanglement becomes nonlocal. The nonlocality is manifested by a new viscous length scale $\delta(w) = (\tilde{\eta}(w)/\gamma)^{1/2}$. The electric field generated by the vortex motion is

$$E_\theta(\rho) = (1/c)B_0 v_\rho + (4\pi\lambda^2 iw/c)j_s. \tag{25}$$

After some manipulation, we have

$$\frac{d}{d\rho}\left(\frac{1}{\rho}\frac{d}{d\rho}(\rho v_\rho)\right) = \frac{c}{B_0}\frac{d}{d\rho}\left(\frac{1}{\rho}\frac{d}{d\rho}(\rho E_\theta)\right) - \frac{4\pi\lambda^2 iw}{B_0}\frac{d}{d\rho}\left(\frac{1}{\rho}\frac{d}{d\rho}(\rho j_s)\right). \tag{26}$$

With the help of Eqs. (25) and (26), Eq. (12) further becomes

$$E_\theta - \delta^2\frac{d}{d\rho}\left(\frac{1}{\rho}\frac{d}{d\rho}(\rho E_\theta)\right) = -\rho_f j_\theta + \frac{4\pi\lambda^2 iw}{c}\left[j_s - \delta^2\frac{d}{d\rho}\left(\frac{1}{\rho}\frac{d}{d\rho}(\rho j_s)\right)\right]. \tag{27}$$

Here the flux flow resistivity $\rho_f = B_0^2/c^2\gamma$ has been introduced. On the other hand, Eq. (12) supplemented by Eq. (2) gives

$$\frac{1}{\rho}\frac{d}{d\rho}\left(\rho\frac{d\,\delta B_z}{d\rho}\right) = \frac{4\pi\gamma}{B_0}\frac{1}{\rho}\frac{d}{d\rho}(\rho v_\rho) - \frac{4\pi\gamma}{B_0}\delta^2\frac{1}{\rho}\frac{d}{d\rho}\left[\rho\frac{d}{d\rho}\left(\frac{1}{\rho}\frac{d}{d\rho}(\rho v_\rho)\right)\right]. \tag{28}$$

By making use of Eqs. (11) and (28), Eq. (10) can finally be, after some calculation, expressed as

$$\frac{\lambda^2\delta^2}{1+\lambda^2\lambda_{nf}^{-2}}\frac{1}{\rho}\frac{d}{d\rho}\left[\rho\frac{d}{d\rho}\left(\frac{1}{\rho}\frac{d}{d\rho}\left(\rho\frac{d\,\delta B_z}{d\rho}\right)\right)\right] - (\delta^2+\lambda_{ac}^2)\frac{1}{\rho}\frac{d}{d\rho}\left(\rho\frac{d\,\delta B_z}{d\rho}\right) + \delta B_z = 0. \tag{29}$$

The solution for δB_z in Eq. (29) can be assumed to be of the form

$$\delta B_z(\rho) = AI_0(\rho/\lambda_1) + BI_0(\rho/\lambda_2), \tag{30}$$

where we have introduced two ac penetration lengths λ_1 and λ_2, and the coefficients A and B will be determined later. Feeding Eq. (30) into Eq. (29), we find

$$\lambda_{1,2}^2 = \frac{1}{2}\left[\lambda_{ac}^2+\delta^2 \pm \left((\delta^2+\lambda_{ac}^2)^2 - \frac{4\lambda^2\delta^2}{1+\lambda^2\lambda_{nf}^{-2}}\right)^{1/2}\right], \tag{31}$$

which is again identical to the ac penetration lengths when the slab is considered [18]. Based on Eqs. (19) and (31) we conclude that the complex ac penetration length seems to be an intrinsic property related solely to the model for vortex dynamics being considered and does not depend on the geometry of the sample and radius of the cylinder or width of the slab. This important feature is also observed in the theory of self-consistent treatment of vortex dynamics as considered by Coffey and Clem [19]. The complex penetration lengths may be dependent on the orientation of the static field generated inside the superconductor as can be seen in Ref. [8]. Nevertheless, it turns out to be also geometry-independent. Eq. (31) reveals that the penetration lengths $\lambda_{1,2}$ are closely related to the flux flow penetration length λ_{ac} in Eq. (19), viscous length δ, normal-fluid skin depth δ_{nf}, and the static London penetration depth λ.

Next, the coefficients A and B in Eq. (30) can be evaluated as follows. By substituting Eq. (30) into Eq. (10) together with $\delta n(\rho = a) = 0$ and the continuity condition $\delta B_z(\rho = a) = \delta H_a$, we obtain the complete expression for $\delta B_z(\rho)$,

$$\delta B_z(\rho) = \frac{\delta H_a}{\lambda_2^{-2}-\lambda_1^{-2}} \times \left((\lambda_2^{-2}-\lambda^{-2}-\lambda_{nf}^{-2})\frac{I_0(\rho/\lambda_1)}{I_0(a/\lambda_1)} - (\lambda_1^{-2}-\lambda^{-2}-\lambda_{nf}^{-2})\frac{I_0(\rho/\lambda_2)}{I_0(a/\lambda_2)}\right). \tag{32}$$

Hence, the corresponding electric field E_θ is given, through Eq. (1), by

$$E_\theta(\rho) = \frac{-iw}{c}\frac{\delta H_a}{\lambda^{-2}-\lambda^{-2}} \times \left[(\lambda_2^{-2}-\lambda^{-2}-\lambda_{nf}^{-2})\lambda_1\frac{I_1(\rho/\lambda_1)}{I_0(a/\lambda_1)} - (\lambda_1^{-2}-\lambda^{-2}-\lambda_{nf}^{-2})\lambda_2\frac{I_1(\rho/\lambda_2)}{I_0(\rho/\lambda_2)}\right]. \tag{33}$$

The associated complex ac permeability is thus directly calculated as

$$\mu(w) = \frac{1}{\lambda_2^{-2}-\lambda_1^{-2}} \times \left[\left(\frac{1}{\lambda_2^2}-\frac{1}{\lambda^2}-\frac{1}{\lambda_{nf}^2}\right)\frac{\lambda_1}{a}\frac{2I_1(a/\lambda_1)}{I_0(a/\lambda_1)} - \left(\frac{1}{\lambda_1^2}-\frac{1}{\lambda^2}-\frac{1}{\lambda_{nf}^2}\right)\frac{\lambda_2}{a}\frac{2I_1(a/\lambda_2)}{I_0(a/\lambda_2)}\right]. \tag{34}$$

It is worthwhile to compare the ac permeability of the slab in the viscous flux liquid, the result is given as [18],

$$\mu(w) = \frac{1}{\lambda_2^{-2}-\lambda_1^{-2}} \times \left[\left(\frac{1}{\lambda_2^2}-\frac{1}{\lambda^2}-\frac{1}{\lambda_{nf}^2}\right)\frac{\lambda_1}{a}\tanh\left(\frac{a}{\lambda_1}\right)\right.$$

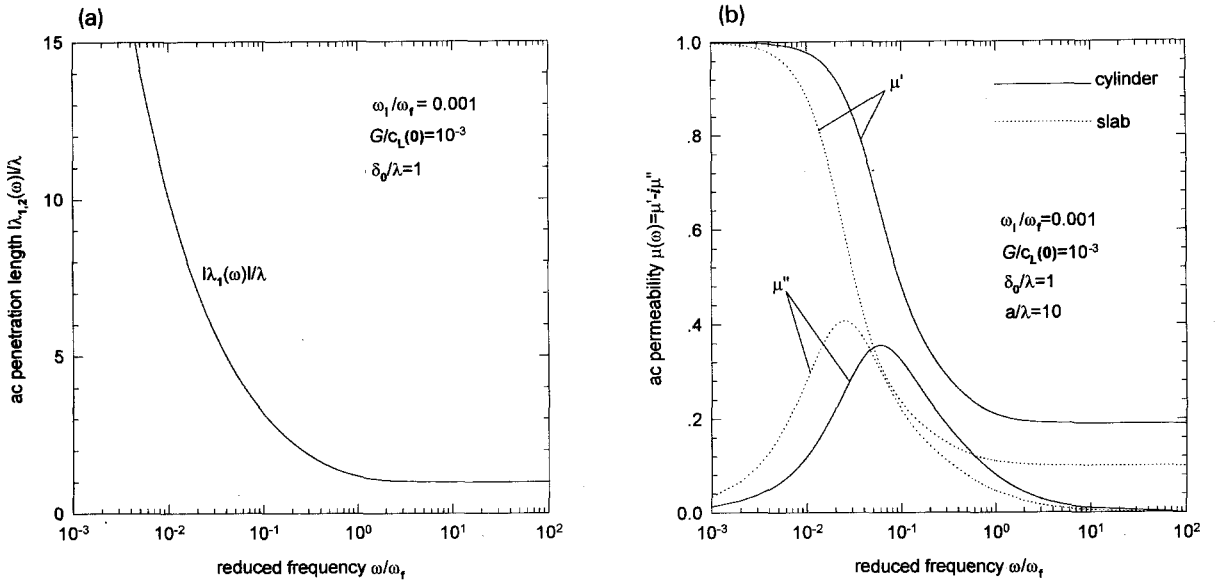

Fig. 3. (a) The normalized complex penetration lengths $|\lambda_{1,2}(w)|/\lambda$ given in Eq. (31) as a function of the reduced frequency w/w_f at $w_\ell/w_f = 0.001$, $G/c_L(0) = 10^{-3}$ and $\delta_0/\lambda = 1$. The $|\lambda_2(w)|/\lambda$ is negligibly small and is not observable. The normal-fluid contribution has been neglected in Figs.3–6. (b) The frequency dependence of complex permeabilities in Eqs. (34) and (35), at $a/\lambda = 10$ and same conditions as in (a).

$$-\left(\frac{1}{\lambda_1^2}-\frac{1}{\lambda^2}-\frac{1}{\lambda_{nf}^2}\right)\frac{\lambda_1}{a}\tanh\left(\frac{a}{\lambda_1}\right)\Bigg]. \tag{35}$$

The coefficients, aside from terms including the dependence on size, are both identical for slab and cylinder (which is reflected in the coefficients A, B described previously). The change in the vortex areal density due to ac field penetration is readily obtained from Eq. (10), we have

$$\delta n(\rho) = \frac{\delta H_a}{\phi_0}\frac{\lambda_f^2}{\lambda_a^2-\lambda_2^2}\left(\frac{I_0(\rho/\lambda_1)}{I_0(a/\lambda_1)}-\frac{I_0(\rho/\lambda_2)}{I_0(a/\lambda_2)}\right). \tag{36}$$

The location ρ_0 where δn reaches a maximum is easily determined, it satisfies the equation

$$I_1(\rho_0/\lambda_1) = \frac{\lambda_1}{\lambda_2}\frac{I_0(a/\lambda_1)}{I_0(a/\lambda_2)}I_1(\rho_0/\lambda_2), \tag{37}$$

which can be numerically evaluated for ρ_0 using the fact that $|\lambda_1| \gg |\lambda_2|$ as described below. The condition for ρ_0 is clearly more complicated than the slab where ρ_0 is approximated at $|\lambda_2|$ [18].

The complex ac permeability and surface impedance of the superconductors are the main quantities used extensively to study the ac response. For a superconductor in the geometry of occupying semi-infinite space, the most relevant element is surface impedance $Z_s = R_s - iX_s$, where R_s is the surface resistance and X_s the surface reactance. For a superconductor in the shape of a cylinder, slab or prism, one usually defers the ac permeability for a theoretical investigation. The role of the imaginary part of the ac permeability is equivalent to the surface resistance, both of them represent the ac dissipation of the superconductor. Similarly, the behavior in X_s is similar to the real part of permeability. From the above results, together with the results reported in the literature [9,12,19,20,22], one concludes that the permeability of a slab or prism varies as a function of the hyper-tangent with complex argument, whereas the cylinder depends on the modified Bessel function, also with complex argument. All the arguments are essentially related with the model-dependent complex penetration length along the sample dimension, as illustrated in Eqs. (34) and (35). These two special functional dependences of the permeabilities for slab and cylinder appeared

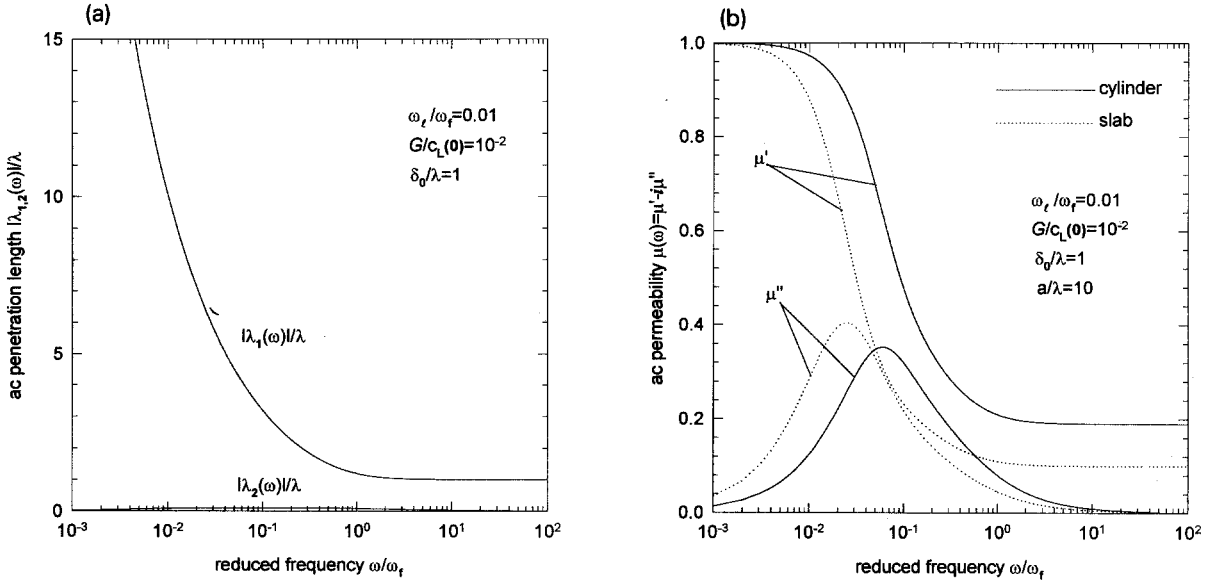

Fig. 4. (a) The normalized complex penetration lengths $|\lambda_{1,2}(w)|/\lambda$ in Eq. (31) at $w_\ell/w_f = 0.01$, $G/c_L(0) = 10^{-2}$ and $\delta_0/\lambda = 1$. The $|\lambda_2(w)|/\lambda$ again is very small. (b) The frequency dependence of complex permeabilities for slab and cylinder at $a/\lambda = 10$ and same conditions as in (a). There is no observable change in the response compared with Fig. 3b.

to show universal behavior. As regards the surface impedance, it is usually described not only in terms of the ac penetration length or the ac resistivity [18]. The primary issue is the related model for vortex dynamics in determining the key result, the complex ac penetration length.

We proceed to examine the effects of viscosity and geomety on the ac permeability of the cylinder in Eq. (34). From Eq. (13), the viscous length $\delta(w)$ is expressed by $\delta(w) = \delta_0(1 + iw\tau_\ell)^{1/2}$ with static viscous length $\delta_0 = \sqrt{\eta_\ell/\gamma}$. In order to analyze the viscous ac response, two frequency scales are introduced [18], namely, $w_\ell = 1/\tau_\ell = G/\eta_\ell$ and $w_\eta = c_L(0)/\eta_\ell$ where w_ℓ describes the relaxation of shear stresses and dominates the length $\delta(w)$, whereas the w_η is the frequency such that $|\lambda_f(w)| \approx \delta_0$. Clearly, both of them decrease with increasing viscosity η_ℓ. Also, the ratio $G/c_L(0) = w_\ell/w_\eta$ will be much smaller than unity for HSTC at the temperature of interest [23].

The frequency w_ℓ significantly indicates the crossover frequency from liquid-like to solid-like response of the vortex lattice. At low frequency $w \ll w_\ell \ll w_\eta$ the dynamics is simply due to flux flow of a vortex liquid. For frequencies $w \gg w_\ell$, the model then describes the flux flow of a vortex solid. As discussed by Chen and Marchetti [18], the only difference between liquid-like and solid-like responses arises from the small difference in the compressional moduli. In Fig. 3a, we plot the ac penetration lengths $|\lambda_1|/\lambda$ and $|\lambda_2|/\lambda$ as a function of reduced frequency w/w_f in conditions of neglecting the normal-fluid contribution $w_\ell/w_f = 0.001$, $G/c_L(0) = 10^{-3}$, and $\delta_0/\lambda = 1$. $|\lambda_2|/\lambda$ is negligibly small and obscure for all frequencies. That is, $\lambda_1(w) \approx \lambda_{ac}$, and $\lambda_2(w) \approx 0$, consequently, the effect of viscosity is very unobservable. The response shown in Fig. 3b is very similar to the Fig. 2a at $w/w_f < 10$.

The disappearance of the second small peak in Fig. 3b is natural, since we have now disregarded the influence of the normal-fluid. The same situation is also observed in Figs. 4a,b, where we have taken $G/c_L(0) = 10^{-2}$ and small viscosity $\delta_0/\lambda = 1$. From the results displayed in Figs. 3 and 4, one is tempted to conclude that the viscous effect may not be observable at very small values of $G/c_L(0)$ and low static viscosity. The difference in response between cylinder and slab is again clearly illustrated in Figs. 3b, 4b. To observe the viscous effect on the permeability, we take $G/c_L(0) = 1$ and $\delta_0/\lambda = 10$ and the results are shown in Figs. 5a,b where the normal-fluid contribution is again ne-

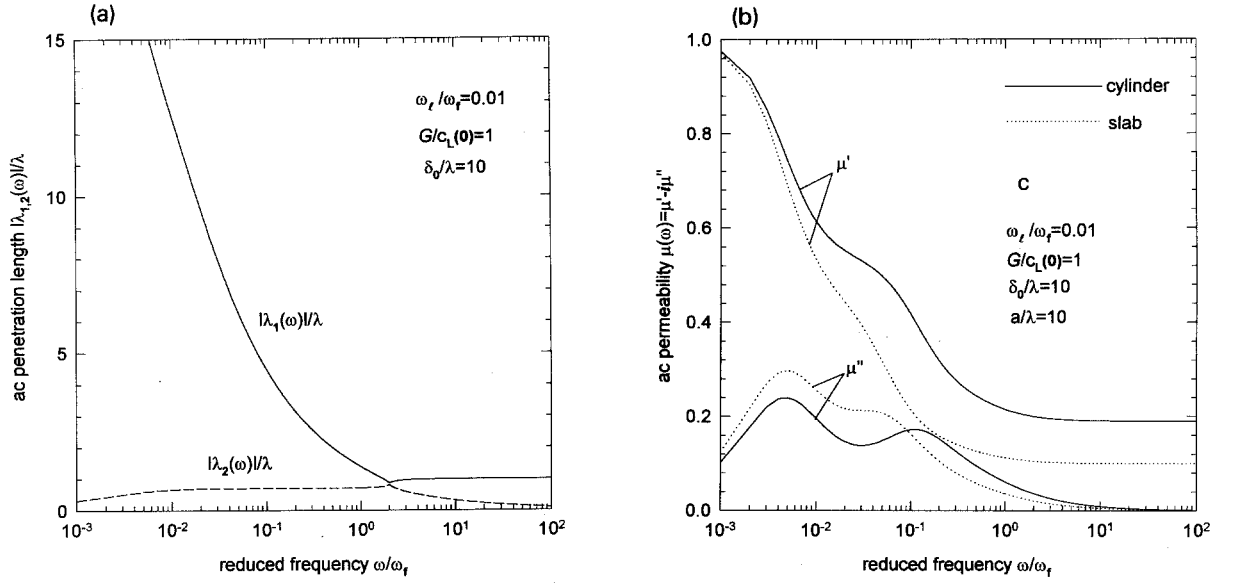

Fig. 5. (a) The complex penetration lengths $|\lambda_{1,2}(w)/\lambda|$ at $w_\ell/w_f = 0.01$, $G/c_L(0) = 1$ and $\delta_0/\lambda = 10$. The $|\lambda_2(w)|/\lambda$ in all frequencies is not observable. (b) The frequency dependence of complex permeabilities for slab and cylinder at $a/\lambda = 10$, $w_\ell/w_f = 0.01$, $G/c_L(0) = 1$ and $\delta_0/\lambda = 10$. A new second peak at very low frequency region is observed because of the large viscosity.

glected. As can be seen, the viscous effect makes λ_2 no longer negligible and is of the order of the static penetration length λ which in turn will impede the flux penetration. Fig. 5a shows that at $w/w_f \ll 10^{-2}$ or $w \ll w_\eta$, $\lambda_1 \approx \lambda_f$ and λ_2 is negligible. For $w/w_f > 10^{-2}$, we have, $\lambda_1 \approx \delta_0$ and $\lambda_2 \approx \lambda$. Therefore, a new second peak occurs at $w \sim w_\eta = 10^{-2} w_f$, as demonstrated in Fig. 5b. The new peak height is larger than the one to the right and has lower peak frequency. Furthermore the peak height has been depressed considerably due to the large viscosity. For much higher frequencies, $w/w_f > 20$, i.e. $w/w_\eta > 200$, the μ'' becomes negligibly small and μ' approaches a constant. The position $w/w_f \approx 20$ in Fig. 5b reveals $\lambda_1 \approx \lambda_2$ indicating that the field penetration is considerably small. In other words, the dissipation in μ'' can be disregarded in the high frequency regime. Concerning the influence of sample geometry, Fig. 5b clearly demonstrates the main features in μ where the two peaks in μ'' are more obvious in the cylinder than in the slab. Also, the variation in μ'' in between the two peaks of μ'' seems to be more pronounced for the cylinder. This again suggests the response depends strongly not only on the complex penetration length but the sample geometry. In Fig. 6a, we consider the case of very large viscosity $\delta_0/\lambda = 100$ and $G/c_L(0) = 10^2$. In this case the crossover occurs around $w/w_f = 10^{-4}$ or $w = w_\eta = 10^{-4} w_f$, where μ'' attains a maximum. The very high viscosity has effectively reenhanced the dissipation peak and makes the peak frequency smaller than that in Fig. 4b by two orders of magnitude. The most important observation is that the peak frequency in this case is almost the same for both cylinder and slab. This can be understood from Fig. 6a where $|\lambda_1| \gg a$ at the crossover frequency and $|\lambda_2| \neq 0$ indicating that the ac field cannot penetrate into the sample due to the viscous screening [18]. Therefore the crossover frequency naturally does not vary with the geometry considered. Nevertheless, the overall magnitudes of the response actually depend on the shape of the sample. As displayed in Fig. 6b, there exists a crossing between μ' and μ'' in the slab at $10^{-4} < w/w_f < 10^{-3}$, while the cylinder does not exhibit this crossing and is fully separated in μ' and μ''.

4. Summary

The linear ac response analysis of the flux-line liquid of the high-T_c superconductor in the shape of a cylinder has been carried out. The complex ac perme-

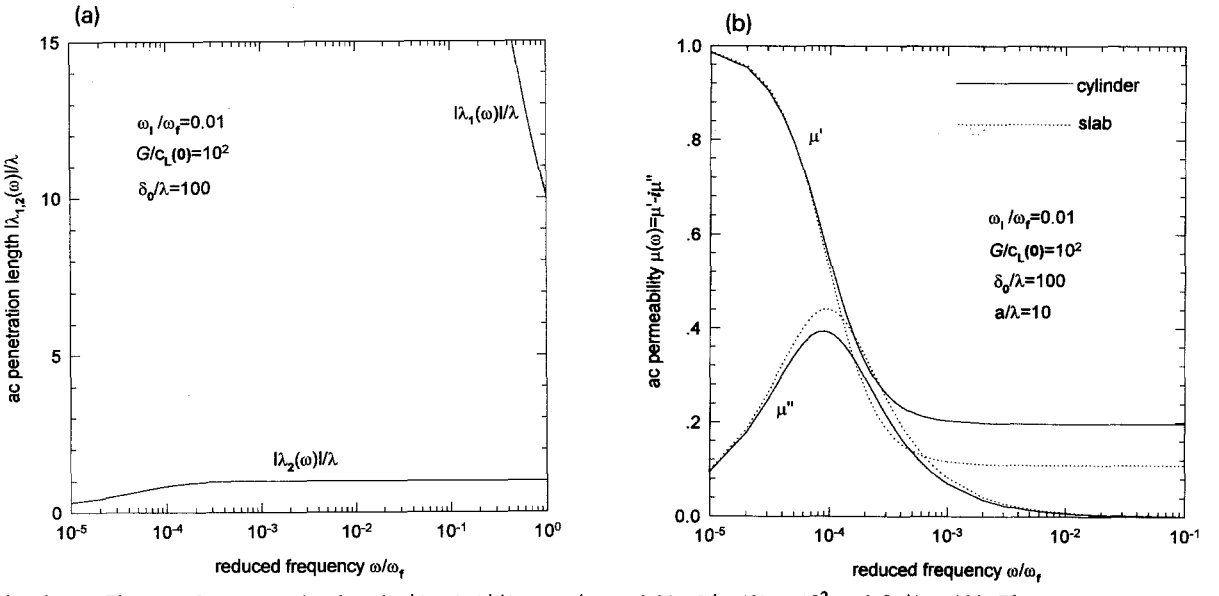

Fig. 6. (a) The complex penetration lengths $|\lambda_{1,2}(w)|/\lambda$ at $w_\ell/w_f = 0.01$, $G/c_L(0) = 10^2$ and $\delta_0/\lambda = 100$. The crossover occurs at $w/w_f \approx 10^{-4}$. (b) The frequency dependence of complex permeabilities of slab and cylinder at $a/\lambda = 10$ and conditions given in (a).

ability for the cylinder is given and comparsion with the slab is also made. In the nonviscous flux liquid, the two peaks in μ'' depend on both the sample geometry and size. The peak located in the lower frequency region indicates the crossover of response from flux liquid to flux solid and the height is decreased for the cylinder. The higher frequency peak arising from the contribution of the normal-fluid is however increased in the cylinder. In the case of the viscous flux liquid, combined with the neglect of the normal-fluid, the response of low viscosity shows some increase in peak height and a shift in peak frequency for the cylinder. For very large viscosity, we find that the peak frequency essentially remains unchanged for both cylinder and slab. The analysis presented here provides some fundamental information about the permeability which is of paramount importance in the arrangement of sample dimension and geometry when experiments are performed.

Acknowledgements

The work is supported by National Scientific Council through No.NSC 85-2112-M009-037 PH.

References

[1] S. de Brion, R. Calemczuk and J.Y. Henery, Physica C 178 (1991) 225.
[2] M.S. Pambianchi, D.H. Wu, L. Ganapathi and S. Anlage, IEEE Trans. Appl. Supercond. AS-3 (1993) 2774.
[3] J. Owliaei, S. Sridhar and J. Tavlvacchio, Phys. Rev. Lett. 69 (1992) 3366.
[4] S. Revenaz, D.E. Oates, G. Dresslhaus and M.S. Dresselhaus, Phys. Rev. B 50 (1994) 1178.
[5] Ph. Seng, R. Gross, U. Baier, M. Rupp, D. Koelle, R.P. Huebener, P. Schmitt, G. Saemann-Ischenko and L. Schultz, Physica C 192 (1992) 403.
[6] M.W. Coffey and J.R. Clem, Phys. Rev. Lett. 67 (1991) 386.
[7] M.W. Coffey and J.R. Clem, Phys. Rev. B 46 (1992) 11757.
[8] M.W. Coffey and J.R. Clem, Phys. Rev. B 45 (1992) 10527.
[9] E.H. Brandt, Phys. Rev. Lett. 67 (1991) 2219.
[10] V.B. Geshkenbein, V.M. Vinokur and R. Fehrenbacher, Phys. Rev. B 43 (1991) 3748.
[11] A.E. Koshelev and V.M. Vinokur, Physica C 173 (1991) 465.
[12] P.H. Kes, J. Aarts, J. van den Berg, C.J. van der Beek and J.A. Mydosh, Supercond. Sci. Tech. 1 (1989) 242.
[13] E.H. Brandt, Z. Phys. B 80 (1990) 169.
[14] N.C. Yeh, Phys. Rev. B 43 (1991) 523.
[15] C.J. van der Beek, V.B. Geshkenbein and V.M. Vinokur, Phys. Rev. B 48 (1993) 3393.
[16] A.P. Malozemoff, T.K. Worthington, Y. Yeshurun and F. Holtzberg, Phys. Rev. B 38 (1988) 7203.

[17] G. Blatter, M.V. Feigel'man, V.B. Geshkenbein, A.I. Larkin and V.M. Vinokur, Rev. Mod. Phys. 1125 (1994) 66.
[18] L.W. Chen and M.C. Marchetti, Phys. Rev. B 50 (1994) 6382.
[19] M.W. Coffey and J.R. Clem, Phys. Rev. B 45 (1992) 9872.
[20] C.E. Gough and N.J. Exon, Phys. Rev. B 50 (1994) 488.
[21] D.S. Fisher, in: Phenomenology and Applications of High-Temperature Superconductor, eds. K.S. Bedell et al. (Addison-Wesley, New York, 1992), p.323.
[22] C.J. Wu and T.Y. Tseng, to be published in Physica C.
[23] E.H. Brandt, Phys. Status Solidi B 77 (1976) 551.